Lund University

division of synchrotron
radiation research

bachelor thesis 15 hp

X-ray diffraction studies on complex metal oxides

Author:
Albin Linder

Supervisor:
Dan Mannix &
Anders Mikkelsen

Spring semester 2015
Examination date: May 20, 2015

LUND
UNIVERSITY

Abstract

The ambition of this project is to assist in the pursuance of understanding the metal to insulator transition found in magnetite at $\sim$120° K. The transition is itself very complex and links together the charge order, orbital order and lattice distortion of magnetite with its magnetic properties. To be able to research these relationships on a more advanced level, synchrotron methods are necessary. For certain experiments it is also desirable to have these thin films without an underlying substrate. The goal of this project is to separate a magnetite thin film from a magnesium oxide substrate and investigate the effects of this process on the structural quality of the film.

Using X-ray diffraction methods a magnetite thin film sample is investigated and its crystal properties are characterized. As the lattice parameter of the magnesium oxide substrate is half of the thin film lattice parameter, the film is found to have very little strain. The quality of the thin film is also established to be high, although the interface between film and substrate seems to be rather rough.

To separate the film from its substrate, chemical etching was attempted. The strategy was to dissolve the substrate leaving behind only the thin film. The plan was then to attach the film on a silicon nitride membrane with a hole in the middle to be able to carry out transmission experiments at a synchrotron. However, the dissolving process proved to be more difficult than expected and the film lift-off process was unsuccessful.

Acknowledgments

I would like to thank my supervisor Danny Mannix for all of your friendly support during this project. You always prioritized me and my project even in the busiest of times, and for that I am truly grateful. It has been fun working with you and I really appreciate the time you have sacrificed for my sake. Thank you.

Additionally, I would like to thank all the nano lab personnel helping out with all lab related things, especially Peter Blomqvist for your patience and quick aid every time the X-ray diffractor broke down, and Ivan Maximov and Håkan Lapovski for your help ordering the necessary chemicals needed in this lab.

I would also like to thank my classmates, Edvin, Felix and Oscar for their invaluable help during our time together here at Lund University. It is because of you guys that I was able to pass all my physics courses. I am also grateful for Björn-Erik's help with some of the XRD measurements as well as his Matlab computational assistance analyzing the data.

Finally I would also like to thank my family and friends for believing in me.

Thank you all!

Table of contents

1 Introduction

Magnetite (Fe_3O_4) is a naturally occurring mineral with ferrimagnetic properties. Its existence and magnetic properties has been known for thousands of years and references to it can be dated as far back as to the sixth century BC in ancient Greece [1]. A highly polarized form of Fe_3O_4 called lodestone can act as an ordinary hand magnet. This fairly strong magnetic material was used in ancient devices such as compasses where it acted as the needle aligning itself to Earth's magnetic field.

The interest in Fe_3O_4 was rekindled in 1939 when E.J.W Verwey discovered that the resistivity in Fe_3O_4 increased abruptly with two orders of magnitude at about 120° K. This temperature is now known as the Verwey temperature T_V and the transition going from a metallic material to an insulating material is called the Verwey transition, or even more general the Metal-Insulator-Transition (MIT). About 70 years after the discovery of the Verwey temperature it was shown using modern synchrotron radiation diffraction, that the transition going from a metallic material to an insulating material could be related to the charge ordering and the orbital ordering[(1)] in the material with respect to the lattice properties. This relation is shown in figure 1. In other words, the Verwey transition is a product of the complex interplay between the charge ordering, the orbital ordering and the lattice order. In addition to this, the magnetic properties of Fe_3O_4 are also thought to contribute to the Verwey transition.

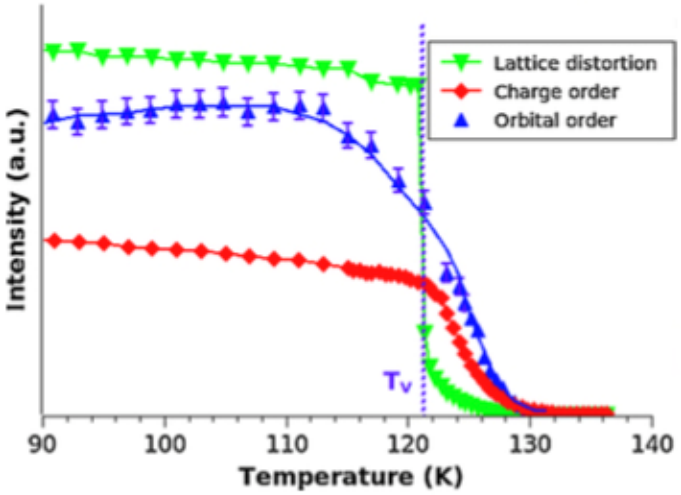

Figure 1: Graph displaying that the lattice distortion, charge order and orbital order all change drastically around the Verwey temperature $T_V \approx 121°$ K. Figure taken from [2].

In recent Magnetic Force Microscopy (MFM) measurements on Fe_3O_4 thin films, a magnetic phase segregation can be shown to occur close to the Verwey temperature. The magnetic moment in the film is pointing in the direction of the surface normal, but near the Verwey transition the magnetic direction is shifted as the well defined magnetic domains suddenly become blurry at the transition depending on the temperature. Further investigation of the relationship between magnetic, charge and orbital order domains in Fe_3O_4 is therefore of great importance in the understanding of this mysterious transition.

[(1)] When electrons in a material interact strongly they can cause charges and electron orbitals to order themselves in a periodic way creating a superlattice.

In order to investigate the co-existence of magnetic domains around the Verwey transition, synchrotron radiation techniques are necessary. With synchrotron methods it could be possible to determine if these magnetic domains separate out into different regions of electronic phase segregation. With a sufficiently focused beam line (obtainable by e.g. MAX-IV) the spatial distribution of the charge, magnetic and orbital properties of Fe_3O_4 thin films could be determined. However, to be able to carry out some of these measurements the Fe_3O_4 thin films will have to be removed from their substrates. The goal of this project is to see how the properties of thin films might change after substrate separation.

1.1 Project overview

In this project a sample consisting of a Fe_3O_4 thin film epitaxially[(2)] grown upon a magnesium oxide (MgO) substrate will be investigated. The strategy is to first evaluate the quality of the thin film by means of X-Ray Diffraction (XRD). This is done by using a X-ray diffractometer (Bruker D8 Discover) found in Lund Nano Lab. The second step is to separate the thin film from the substrate. This procedure is done by chemically dissolving the substrate with an ammonium sulphate-solution. Finally, the thin film is to be re-measured without the substrate in order to see how the separation process has affected the film.

2 Theory

Pure eyesight is not sufficient to qualitatively study the microscopic world. In order to observe smaller objects than we can see, we turn to microscopes, that have better resolving power than our eyes. But there is a limitation in the resolving power of microscopes as well, namely the wavelength of the light used in microscope measurements. In order to go smaller and resolve solid structures on an atomic level, the measured light must have a wavelength comparable to the atomic spacings of the structure. Light which fulfills this requirement are found in the X-ray region of the electromagnetic spectrum. By the theory of X-Ray Diffraction (XRD) it is possible to observe how the atoms in solids are arranged. The following theory sections will provide the reader with the basic XRD theory used in this project.

2.1 X-ray scattering

In this section, X-ray scattering processes will be briefly explained. Although X-ray scattering does not follow classical theory, a classical approach will still be considered with only elastic scattering, which simplifies calculations considerably. For a more detailed explanation regarding X-ray scattering processes please read chapter one in B.E Warren's book *X-ray diffraction* [3].

X-rays can be scattered against charged particles such as electrons. In this process the rays will change their direction of propagation and if there is no change in momentum, as in Thomson scattering, the wavelength will remain the same before and after the interaction. A change in wavelength may however occur if the process is inelastic such as a Compton scattering event. In this project only Thomson scattering will be considered as

[(2)] See section 3.1.3 Epitaxial growth on page 12.

Compton scattering, which due to its incoherence, does not contribute to the creation of *Bragg peaks* (later to be defined).

Because X-rays are a part of the electromagnetic spectrum they consist of electric and magnetic fields in oscillations perpendicular to the direction of propagation of the ray. Therefore, if we consider an unpolarized X-ray beam traveling through space along the x-direction, its electric field will be in an arbitrary direction in the yz-plane. If this beam is incident on a free single electron it will exert a force on the electron parallel to the electric field. This force will hence accelerate the electron in the yz-plane making it oscillate along the direction of the electric field. When a charged particle is accelerated it will radiate light according to electromagnetic theory and the considered electron will thus begin to radiate. The initial beam is said to be scattered against the electron, producing radiation which spreads out in different directions.

2.2 Crystal structure

When atoms arrange themselves into solids they do so by settling down into positions with as low potential energy as possible, i.e. with as much binding energy as possible. For different elements/molecules certain geometrical arrangements are therefore more beneficial to align in than others. If the arrangement for a set of closely positioned atoms repeats itself over a large distance we call it a crystal.

In order to describe a crystal we need a translational mechanism known as a lattice. A lattice is a three dimensional array which repeats itself over space. The idea of introducing the concept of a lattice is to be able to explain where atoms are placed in a crystal. The atoms themselves are said to constitute the basis of the crystal. The basis is however not exclusively given by just atoms, it could also be given by complex molecules and even protein.

In other words, a simple explanation of a lattice and a basis is that a lattice is a mathematical concept which tells you where to "put" the atoms and a basis decides what atoms to use in a crystal. For more information regarding crystal structures we refer to chapter 2 in [3], chapter 2 in [4] and chapter 2 in [5].

2.2.1 Real space crystal lattice

In order to describe a crystal structure a so called lattice is used. In real space a lattice is an array of points in which the atoms are located. A commonly used lattice is the *Bravais lattice* which is mathematically defined as:

$$\mathbf{R}_{mno} = m\mathbf{a_1} + n\mathbf{a_2} + o\mathbf{a_3}$$

where $\mathbf{a_{1,2,3}}$ are three non-colinear vectors composing the lattice ($\mathbf{a_{1,2,3}}$ are also called the crystal axes), m,n,o are integers that give the position of an atom positioned at $\mathbf{R}_{mno}$, measured from a convenient origin at one of the lattice points. The Bravais lattice thus defines points where atoms are located by a set of non co-linear lattice vectors. With the lattice it is possible to construct a so called unit cell. A unit cell is a volume of space which, when translated through the lattice vectors, fills space without overlaps or leaving

behind voids. A primitive unit cell contains one atom but in many cases non-primitive unit cells are more convenient to use [4]. In figure 2 a simple cubic (SC) and a face centered cubic (FCC) unit cell are illustrated.

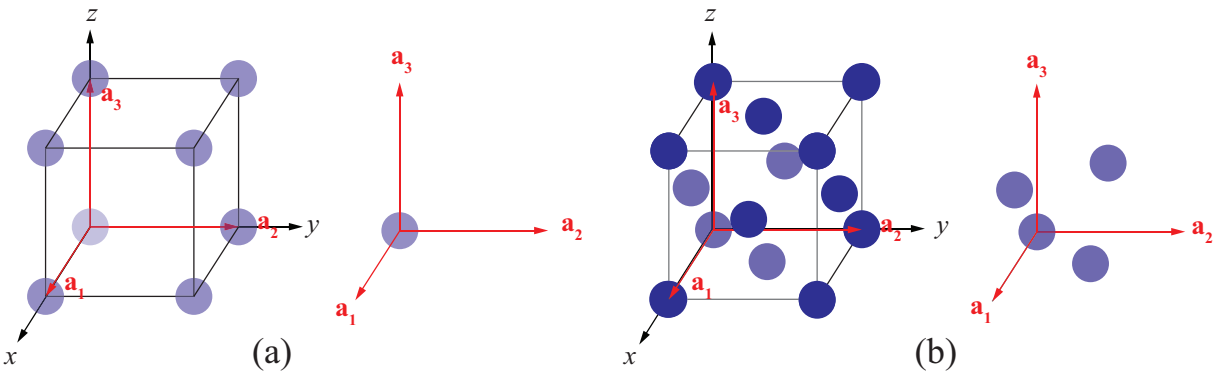

Figure 2: In (a) a simple cubic unit cell is shown. The SC unit cell is a primitive unit cell as it only has one atom. The translational lattice vectors are also shown where the atom sits in the origin. In (b) a non-primitive FCC unit cell with the same dimensions and same lattice vectors as (a) is shown. The unit cell here has 4 atoms shown in (b).

2.2.2 Reciprocal lattice

The concept of the *reciprocal lattice* is vital to XRD theory as it determines how the periodic real space lattice interacts with waves [6]. A reciprocal lattice $\mathbf{G}$ is, similarly to the real space lattice, also given by a Bravais lattice:

$$\mathbf{G}_{m'n'o'} = m'\mathbf{b_1} + n'\mathbf{b_2} + o'\mathbf{b_3}$$

where $\mathbf{b_{1,2,3}}$ are the reciprocal lattice vectors and m', n', o' are integers. The reciprocal lattice maps out lattice points in the imaginary reciprocal space which relates to real space through a Fourier transformation. The condition for defining the reciprocal lattice is that it has to fulfill the following condition:

$$e^{i(\mathbf{R}\cdot\mathbf{G})} = 1 \qquad \Longleftrightarrow \qquad \mathbf{R}\cdot\mathbf{G} = 2\pi n, \qquad n \in \mathbb{Z}$$

This condition will automatically be fulfilled by defining the reciprocal lattice vectors $\mathbf{b_{1,2,3}}$ as:

$$\mathbf{b_1} = 2\pi\frac{\mathbf{a_2}\times\mathbf{a_3}}{\mathbf{a_1}\cdot(\mathbf{a_2}\times\mathbf{a_3})}, \qquad \mathbf{b_2} = 2\pi\frac{\mathbf{a_3}\times\mathbf{a_1}}{\mathbf{a_1}\cdot(\mathbf{a_2}\times\mathbf{a_3})}, \qquad \mathbf{b_3} = 2\pi\frac{\mathbf{a_1}\times\mathbf{a_2}}{\mathbf{a_1}\cdot(\mathbf{a_2}\times\mathbf{a_3})}$$

From these expressions one can derive the following:

$$\mathbf{a_i}\cdot\mathbf{b_j} = 2\pi\delta_{ij}$$

where δ_{ij} is Kronecker's delta that is 1 for $i = j$ and zero otherwise. A long vector in real space will hence generate a short vector in reciprocal space and vice versa. The length of the reciprocal lattice vectors ($a_i = |\mathbf{a_i}|$, $b_i = |\mathbf{b_i}|$) defines the reciprocal lattice units (r.l.u):

$$b_i = \frac{2\pi}{a_i}$$

2.2.3 Lattice planes and Miller indices

In Euclidean space a plane is uniquely determined by three non-colinear points. Thus, by connecting three non-colinear points in a Bravais lattice a so called lattice plane can be defined. Because of the translational symmetry and periodic nature of a Bravais lattice the plane will contain infinitely many points. Through this symmetry it is also possible to contain all lattice points by assembling a set of equidistant parallel lattice planes stacked on top of each other. The whole set of these planes can therefore be determined by defining one normal vector to one of these planes.

In order to define the direction of lattice planes, *Miller indices* are used. These are denoted by integer values h, k, l and form a vector in reciprocal space which is orthogonal to the considered lattice plane in real space, i.e. a normal vector to the lattice plane. The vector in reciprocal space is thus given by $h\mathbf{b_1} + k\mathbf{b_2} + l\mathbf{b_3}$. By this definition the lattice plane will intersect the real space lattice axes at multiples of $\mathbf{a_1}/h$, $\mathbf{a_2}/k$ and $\mathbf{a_3}/l$. The purpose of Miller indices is to be able to define directions within a unit cell. These planes are important to define as they will help determining the lattice plane spacings which are used to find *Bragg reflections*. Examples of Miller indices defining lattice planes are shown in figure 3.

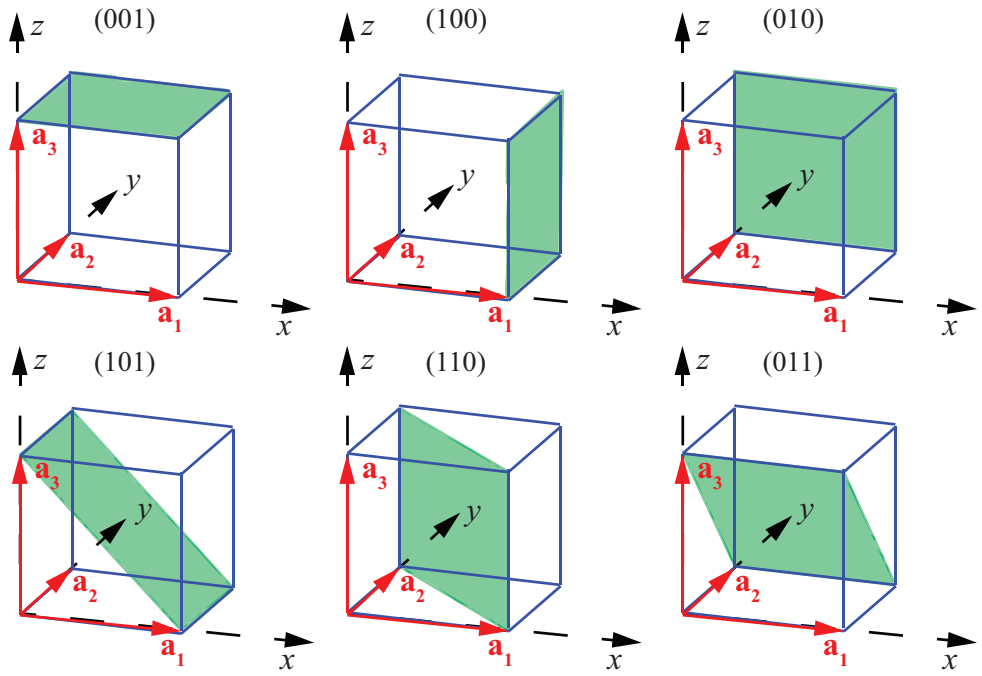

Figure 3: Examples of Miller indices determining different lattice planes.

The directions of the vectors $\mathbf{b_1}$, $\mathbf{b_2}$ and $\mathbf{b_3}$ will later, when analyzing the data, be referred to as the H, K and L-directions respectively. These directions (H, K and L) are given in capital letters in order to distinguish them from the Miller indices (hkl). HKL will, i.e. define directions in reciprocal space while a set of hkl will define a specific lattice plane. The reflection from a certain plane will also be described by using hkl.

2.3 Laue equations

The Laue equations set up conditions which have to be obeyed in order to generate constructive interference for elastic scattering in XRD measurements.

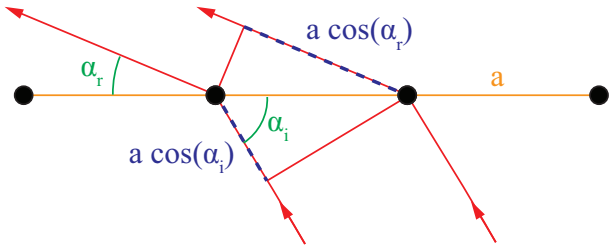

Figure 4: Relation between incident and diffracted beams.

Consider incident X-ray beams at an angle α_i on two atoms where the distance between the atoms is a, as shown in figure 4. The light gets scattered by the atoms and reflected at an angle α_r, but because of the spacing between the atoms there will be a path difference for the diffracted light. If the path difference PD between the scattered beams is a multiple of the wavelength of the light, there will be constructive interference. The constructive diffraction condition therefore becomes:

$$PD = n\lambda \qquad \text{where} \qquad n \in \mathbb{Z} \tag{1}$$

$$\implies a(\cos\alpha_i \pm \cos\alpha_r) = n\lambda \tag{2}$$

In the case of a three dimensional lattice there are two additional dimensions that also must fulfill eq.(2). The constructive diffraction condition for the three translational directions a_1, a_2, a_3 then becomes:

$$a_1(\cos\alpha_i \pm \cos\alpha_r) = h\lambda \tag{3}$$
$$a_2(\cos\beta_i \pm \cos\beta_r) = k\lambda \tag{4}$$
$$a_3(\cos\gamma_i \pm \cos\gamma_r) = l\lambda \tag{5}$$

where $\alpha_{i,r}$, $\beta_{i,r}$ and $\gamma_{i,r}$ are incident/reflected angles in a_1, a_2, a_3 directions and h, k, l have to be integers to fulfill eq.(2). These equations are the Laue equations for constructive diffraction.

The magnitude of a wave vector $\mathbf{k}$ for electromagnetic waves is inversely proportional to the wavelength λ of the wave as $\mathbf{k} = 2\pi/\lambda$. If the wave gets reflected through a Thomson scattering event, the magnitude of the incident wave vector $\mathbf{k_i}$ would be the same as the reflected wave vector $\mathbf{k_r}$, as λ in such an event is unaltered. To describe a scattering event it is common to use the scattering vector $\mathbf{Q}$ which is defined by the vector difference between the two wave vectors, $\mathbf{Q} = \mathbf{k_r} - \mathbf{k_i}$. The Laue equations can also be expressed in terms of $\mathbf{Q}$ as [7]:

$$\mathbf{Q} \cdot \mathbf{a_1} = h \tag{6}$$
$$\mathbf{Q} \cdot \mathbf{a_2} = k \tag{7}$$
$$\mathbf{Q} \cdot \mathbf{a_3} = l \tag{8}$$

where the scalar product between the scattering **Q** and the lattice vectors are equal to the Miller indices.

For orthorhombic unit cells (all unit cells where the lattice vectors are perpendicular to each other) the lattice planes defined by the Miller indices will be separated by a distance d_{hkl}. This distance will for orthorhombic unit cells have the following relation:

$$\frac{1}{d_{hkl}^2} = \frac{h^2}{a_1^2} + \frac{k^2}{a_2^2} + \frac{l^2}{a_3^2} \tag{9}$$

2.4 Bragg's law

The Braggs, father and son, studied and analyzed crystal structures by means of X-rays. In 1912 they were together able to derive a powerful equation called *Bragg's law* which still is fundamental in XRD studies. With Bragg's law it is possible to determine the different crystal lattice plane spacings and thus also its lattice parameters. For their work in the XRD field they were both rewarded the Nobel prize in physics in 1915 [8].

2.4.1 Bragg's law for symmetric reflections

As the atoms in a crystal are arranged in lattice plane layers assembled on top of each other the X-rays can be assumed as being scattered by the lattice planes themselves. This is of course a rough simplification of the problem and it might not have much physical justification but this approximation is highly successful and commonly used. The Bragg's law condition is of great importance in all XRD studies and will be used in this project as a powerful tool necessary for structure analysis.

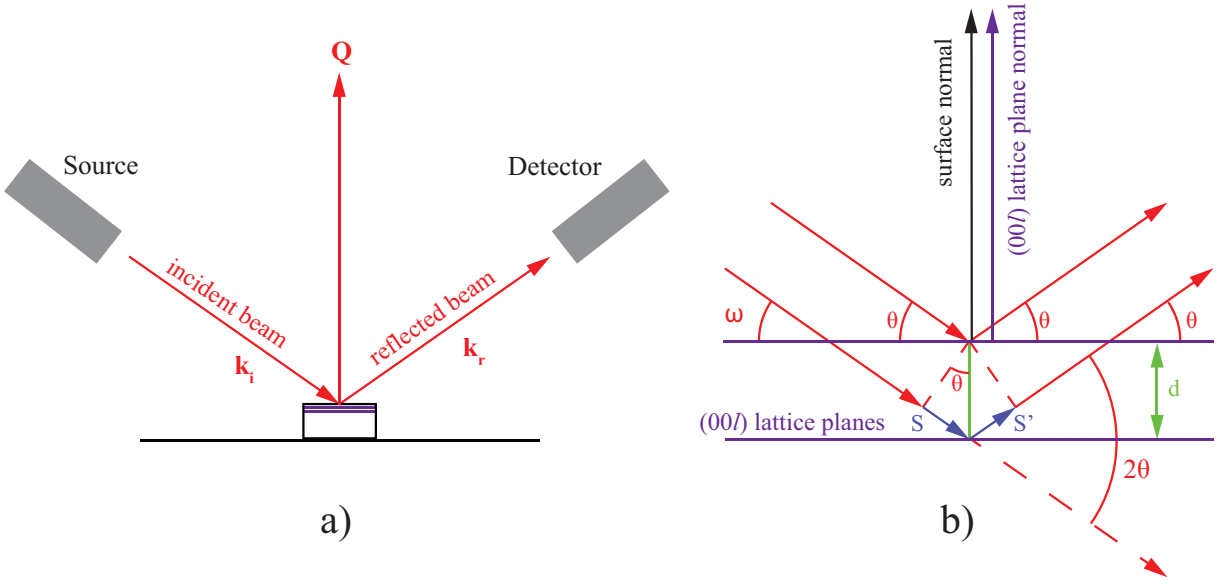

Figure 5: (a) Macroscopic view of XRD by a specular reflection (00l) and, (b) the microscopic view of the X-rays being scattered against two adjacent lattice plane layers. Here the Bragg angle θ is equal to the measured angle ω

The derivation of Bragg's law is usually done by simple geometry. In figure 5, a collimated monochromatic X-ray beam is incident upon two lattice planes at an incident angle of θ

and the planes are separated by a distance d. The beam gets scattered by the two planes but because of the separation between the planes there will be a path difference between the two beams when they coincide at infinity[3]. The total path difference then becomes $S + S'$. By combining this together with the condition for constructive interference (eq. (1)) we can derive Bragg's law by using the law of sine to calculate S and S':

$$S + S' = n\lambda \quad \Longleftrightarrow \quad d\sin\theta + d\sin\theta = n\lambda \quad \Longleftrightarrow \quad 2d\sin\theta = n\lambda \tag{10}$$

In XRD measurements there will be pronounced peaks in intensity wherever eq. (10) is fulfilled. These well defined peaks are called *Bragg peaks*. As the wavelength is fixed for the XRD equipment used in this project and the measured variable is the angle ω ($=\theta$) the atomic spacing d can be calculated. By knowing d the lattice parameters can then successively be deduced.

The reflection in figure 5 is symmetric which means that the incident angle is equal to the reflected angle. In practice the Bragg angle θ is not measured directly as there always will be small offsets to this angle[4]. The Bragg angle θ can always be determined by $\theta = 2\theta/2$. The measured angle is however ω which in a symmetric reflection is equal to θ. This is not the case in asymmetric reflections.

2.4.2 Bragg's law for asymmetric reflections

In XRD studies the sample under investigation usually has a flat surface on which the X-ray beam is incident upon. The surface plane can thus be used as reference when rotating the sample in order to find a certain Bragg peak. The rotations of the sample is then relative to the surface of the sample. But if the lattice plane under inspection is not parallel to the flat surface of the sample, an offset angle will arise which must be taken into account in order to find the Bragg peak corresponding to that specific lattice plane. Figure 6 graphically shows the offset angle α as the angle between the plane normal of the inspected lattice plane and the plane normal of the sample surface.

[3] Because the atomic scale is of the order of $\sim$1Å the detector can be approximated to be located at infinite distance from the origin of the scattering event.

[4] These offsets could for example be due to small deviations in aligning the experimental setup etc. In theory there is however no offsets in the case of symmetric reflections.

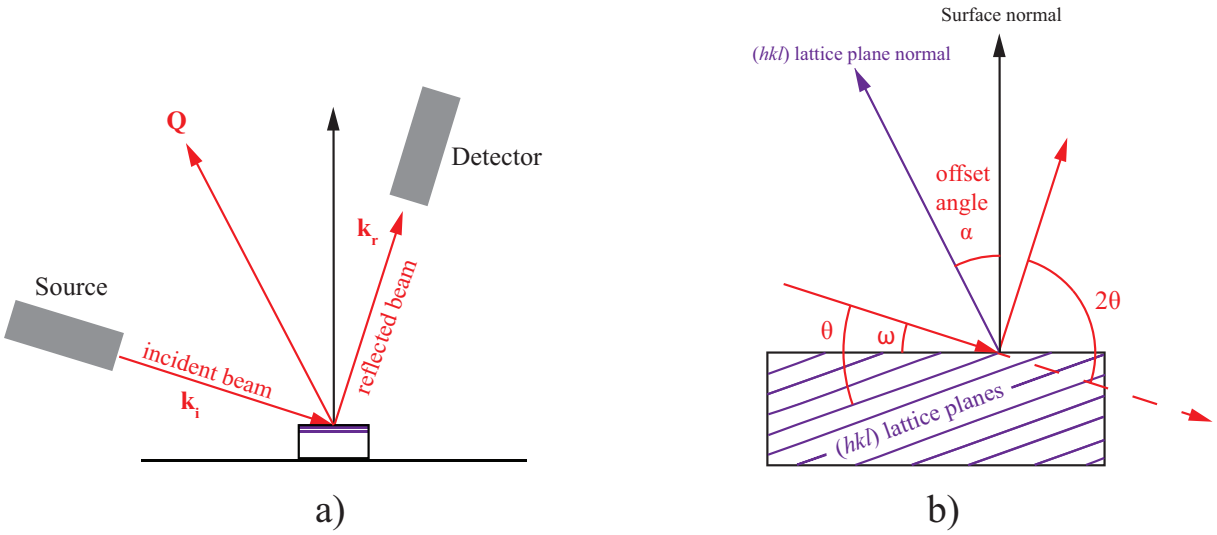

Figure 6: (a) Macroscopic view of a asymmetric (hkl) reflection. (b) A microscopic view of the reflection where Bragg angle $2\theta/2$ is greater than ω.

The measured angle ω is the angle between the incident beam and the surface of the sample while 2θ is the angle of change for the reflected beam. This means that if the beam is reflected by a lattice plane that is not parallel to the sample surface plane then:

$$\frac{2\theta}{2} \neq \omega \qquad \text{but rather} \qquad \frac{2\theta}{2} = \alpha + \omega$$

The symmetric reflection is only valid when the lattice plane normal is parallel to the surface normal of the inspected crystal. Examples fulfilling this criteria in our case is all $(00l)$ Bragg peaks. But for other Bragg peaks such as $(h0l)$, $(0kl)$ or (hkl) where $h, k, l \neq 0$ the normal Bragg's law must be modified to account for an offset that arises in θ. The reason for the upcoming of this offset is because the incident angle is measured from the surface plane of the crystal and not from the plane under inspection. In the $(00l)$ Bragg peak case these two planes are parallel and therefore no offset has to be taken into account.

2.5 Film thickness

A thin film is, as its name suggests, a crystalline structure which is restrained in one dimension, arbitrarily chosen to be along the $\mathbf{a_3}$ crystal axis. The in-plane crystal axes $\mathbf{a_1}$ and $\mathbf{a_2}$ can however be thought to be infinite as there are no restrictions in how wide and long a thin film can be. As there is a restrained thickness of the film in $\mathbf{a_3}$ the diffracted intensity in reciprocal space will also be affected along L. The intensity profile for a Bragg peak along L will show a succession of maxima and minima[(5)]. These maxima and minima form fringes which arise from the interference of the waves scattered at the two interfaces of the film (the surface of the film and the film to substrate interface). The fringes have therefore nothing to do with the crystalline structure of the sample. The distance between two consecutive fringes (e.g. distance between adjacent maxima) measured in q (magnitude of the scattering vector $|\mathbf{Q}|$) is inversely proportional to the

[(5)] These maxima and minima are called Kiessig fringes and can be further read about in [7]

film thickness T_{fringe} [7]. These are features of the so called Laue oscillations. The film thickness T_{fringe} is given by:

$$T_{fringe} = \frac{1}{\Delta q} \qquad \text{where} \qquad \Delta q = q_i - q_{i-1} \tag{11}$$

where q_i is the momentum transfer of a maximum and q_{i-1} is the momentum transfer of the previous maximum. If the Bragg angle θ and the wavelength λ is known, a convertation to q is given by:

$$q = 4 \sin\theta / \lambda \tag{12}$$

The widths of the Bragg peaks are related to a length-scale referred to as the correlation length, i.e. the length over which the scattering from the atoms is coherent. For a perfect crystal, the widths of the Bragg peaks will be infinetely sharp, essentially representing the resolution of the X-ray diffraction equipment in the directions H, K and L. However, when the thickness of the crystal is finitely limited in one direction as in the case of a thin film, the width of the Bragg peaks perpendicular to the film surface (in our case L-direction) become much broader and reflect the finite thickness of the film. The measured width Λ of the film Bragg peaks, given in FWHM, can thus be used to estimate the film thickness T_{fwhm} as:

$$T_{fwhm} = \frac{1}{\Lambda} \tag{13}$$

2.6 Calculations

By combining eq. 9 with Bragg's law eq. (10), the lattice parameters can be calculated. For a symmetric reflection, i.e. a $(00l)$ reflection, the length of $\mathbf{a_3}$ is given by:

$$a_3 = \frac{l\lambda}{2\sin\theta} \tag{14}$$

and by knowing a_3, a_1 can for a $(h0l)$ reflection be calculated as:

$$a_1 = h\left(\left(\frac{2\sin\theta}{\lambda}\right)^2 - \frac{l^2}{a_3^2}\right)^{-1/2} \tag{15}$$

Analogously a_2 can be calculated from a $(0kl)$ reflection as:

$$a_2 = k\left(\left(\frac{2\sin\theta}{\lambda}\right)^2 - \frac{l^2}{a_3^2}\right)^{-1/2} \tag{16}$$

For derivations of these relations, see appendix A.

2.7 Structure factor

The structure factor is a mathematical description for how light scatters by a unit cell. For a given hkl-reflection the structure factor can be used in order to see how strong the reflection is as its square is proportional to the intensity of the scattered light. Depending on the structure of the lattice, the structure factor also sets up certain selection rules for which reflections are allowed and which are not due to constructive and/or partial

destructive interference of the scattered waves.

When a crystal is irradiated by monochromatic X-ray radiation Thomson scattering will take place by the atoms positioned at the lattice points. Thomson scattering is an elastic scattering process where the incoming energy of the photon is the same as the outgoing energy. The only thing that changes is the direction of the photon. In XRD studies only Thomson scattering is of interest because only unmodified scattering gives rise to Bragg reflections. Modified scattering, such as Compton scattering, is completely incoherent due to the change in wavelength and thus only creates a diffuse background [3].

When a unit cell contains more than one atom not all reflections may give constructive interference for any given hkl plane. The atomic positions in a unit cell is given by (xyz) co-ordinates from a suitable origin, see figure 2. The waves scattered by different atoms in the unit cell are combined in order to find the phase difference between each of them and a scattered wave at the origin. Constructive interference for a hkl reflection can only occur when the translations a, b, c involves phase changes of $2\pi h$, $2\pi k$ and $2\pi l$. This implies that the total phase change from the origin to the atom at (xyz) is:

$$2\pi \left(h\frac{x}{a} + k\frac{y}{b} + l\frac{z}{c} \right)$$

This can be rewritten with fractional co-ordinates as:

$$2\pi(hu + kv + lw)$$

where $u{=}x/a$, $v{=}y/b$ and $w{=}z/c$. The scattering factor f for each of the atoms multiplied by its corresponding phase factor defined above results in its contributing reflective amplitude. The structure factor $F(hkl)$ is given by sum of all these products:

$$F(hkl) = \sum_{n}^{N} f_n \cdot e^{2\pi i(hu_n + kv_n + lw_n)} \tag{17}$$

where the index n corresponds to the different atoms and N is the total number of atoms in the unit cell. The strength of the scattering factor relates to the number of electrons in the atom and it therefore changes with elements. The intensity of the diffracted beam is proportional to the square of the structure factor, i.e. $I \propto |F(hkl)|^2$ according to [3].

3 Methodology

3.1 Samples

A thin film is a crystal layer attached on top of the surface of another crystal structure. The thickness of a thin film is in the range of a few Ångstöms up to several micrometers. The thin film in our case is made up of magnetite (Fe_3O_4) epitaxially grown on a magnesium oxide (MgO) substrate by pulsed laser deposition. The size of the sample is approximately 5mm×3mm×1mm.

3.1.1 Magnetite Fe_3O_4

Fe_3O_4 has a cubic lattice structure which means that the lattice parameters a_1, a_2, and a_3 are all of equal length and orthogonal with respect to each other. The lattice parameter, i.e. the length of $\mathbf{a_1}$, $\mathbf{a_2}$, and $\mathbf{a_3}$, is 8.398 Å. Although Fe_3O_4 has a cubic unit cell, the unit cell is still rather complex. The oxide anions are arranged in a FCC lattice while the iron cations occupy octahedral and tetrahedral sites in the lattice. As the lattice composing a crystal will determine which Bragg reflections are allowed, there will be restrictions on what Miller indices will be able to generate a constructive reflection. The allowed Miller indices for Fe_3O_4 have to obey the selection rules given in table 1 [9].

Table 1: These selection rules apply for crystals of space group $Fd\bar{3}m$ No. 227, such as Fe_3O_4, and determine the allowed Bragg reflections depending on the given Miller indices.

Reflection	**Selection rule**	**Reflection**	**Selection rule**
hkl	$h+k$, $k+l$, $h+l=2n$	$0kl$	k, $l=2n$, $k+l=4n$
$h0l$	$h+l=2n$	$hk0$	h, $k=2n$, $h+k=4n$
hhl	$h+l=2n$	hkh	$h+k=2n$
hkk	$h+k=2n$	$h00$	$h=4n$
$0k0$	$k=4n$	$00l$	$l=4n$
$0kk$	$k=2n$	$h0h$	$h=2n$
$hh0$	$h=2n$	-	-

3.1.2 Magnesium oxide MgO

A thin film of Fe_3O_4 is grown upon a magnesium oxide (MgO) substrate. The reason why MgO is used as a substrate is because, like Fe_3O_4, it has a cubic lattice with a desirable lattice parameter length of 4.213 Å which is half of the lattice parameter of Fe_3O_4. Because of this the film should match and be able to fit the lattice of MgO rather well at the boundary.

Since MgO has a face-centered-cubic (FCC) crystal lattice the restrictions in Miller indices for allowed reflections are easily derived from the structure factor (see appendix A). The resulting selection rules then states that the allowed hkl for a FCC lattice has to be either all even or all odd (where 0 counts as an even integer).

3.1.3 Epitaxial growth

The Fe_3O_4 thin film sample used in this lab was grown in Germany at Technische Universität München. The method used to grow these kinds of samples is through Pulsed Laser Deposition (PLD) which is a powerful method to fabricate epitaxial thin films on complex oxides. There are three parts in the PLD process; (i) vaporization of the target material, (ii) transportation of the vapor plume to the substrate, and (iii) the growth of thin films on the substrate.

In the vaporization process (i) high energy laser pulses are focused on a polycrystalline target. The energy density at the target surface is regulated by a system of optical lenses and can be altered in order to evaporate surface atoms of the target. This will create a plasma plume containing the desired particles. The plasma plume is then transported to the substrate (ii) where it is adiabatically cooled down. Because the plume still contains particles with high kinetic energies it is further thermalized by adding a background gas. The collisions between the plume particles and this background atmosphere will further thermalize the plume. In oxide materials O_2 is often used as the background gas. The reason for this is to compensate for possible oxygen vacancies in the thin films due to sputtering processes produced from the high energy particles in the plasma. The last process (iii) is the actual epitaxial thin film growth on the substrate. This process is due to several microscopical processes, such as adsorption, diffusion and desorption of adatoms. All these processes are dependent on the kinematics of the system determined by the deposition rate, substrate temperature and background pressure [10].

3.2 Bruker D8

In this project a Bruker D8 Discover X-ray diffractometer was used. The Bruker D8 Discover is an instrument built for XRD. It consists of three essential parts; (i) a X-ray tube producing a monochromatic X-ray beam, (ii) a sample stage which is rotatable- and movable in three dimensions, and (iii) a circularly movable detector in the horizontal plane. An overview picture of the equipment and these three parts is shown in figure 7.

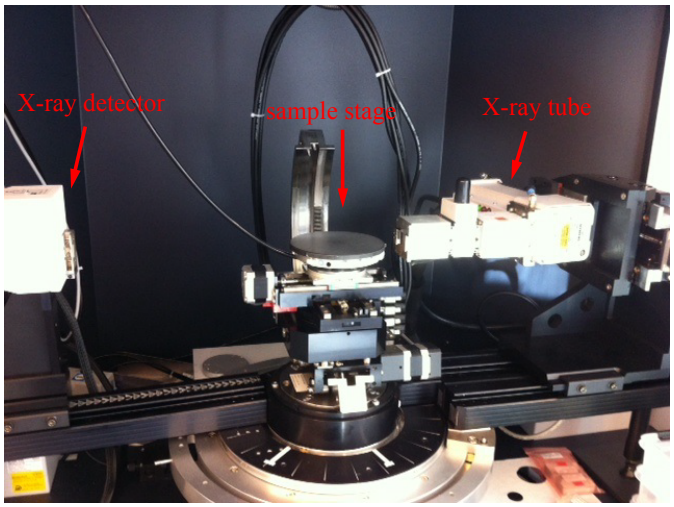

Figure 7: Image of the used Bruker D8 Discover X-ray diffractometer.

The sample of investigation is placed upon the sample stage and is irradiated by the monochromatic X-ray beam produced by the X-ray tube. The crystal structure of the sample will create a diffraction pattern with sharp maxima at certain angles. If the incident beam from the X-ray tube and the diffracted beam from the sample together fulfills the Bragg condition where the detector is positioned, a high count of X-rays can be measured indicating very high intensity. But if the Bragg condition is not fulfilled there will be almost no measurable intensity. In order to fulfill the Bragg condition the sample stage is rotatable around all axes and the detector itself can be rotated horizontally.

Where the Bragg condition is fulfilled a Bragg peak will arise. In the vicinity of this peak the intensity can change drastically by changing the Bragg angles by very small increments. The measured intensities can then be used to make so called line scans or mesh scans given in reciprocal space for the crystal. Further explanation of this will be given in the result section.

3.2.1 The X-ray tube

In order to produce X-rays the Bruker D8 is equipped with a X-ray tube. Inside the X-ray tube a filament is heated inside a vacuum tube making it emit electrons. These free electrons are then accelerated towards a copper (Cu) target anode. When the target gets bombarded by high energy electrons the core Cu-electrons (K-shell electrons) get knocked out leaving behind a vacancy for higher shell electrons to jump down to. The most common transitions is for L- and M-shell electrons to jump down to the empty energy level, i.e. the K_α and K_β transition lines. In order to separate the desired K_α[(6)] from the K_β line to create a monochromatic X-ray beam, Göbel mirrors are used [11]. Göbel mirrors are monochromating mirrors which, for a certain direction, only fulfill the Bragg condition for a specific λ and θ. The K_β line can thus effectively be removed from the desired K_α line. The beam is then collimated using Montel optics [11] before exiting the tube.

3.2.2 Sample stage and X-ray detector

One important part of the Bruker D8 instrument is the sample stage where the sample under investigation is mounted. The sample is then held in place by small vacuum pumps. The sample stage is rotatable around all three xyz-axes and it is also translationally movable along these axes. The X-ray tube is, in our case, immovable and can only create a collimated X-ray beam in a fixed direction (y-direction in figure 8) and the detector can only be moved in a circular path around the sample stage. But as the orientation of the sample is crucially important in order to fulfill the Bragg condition in a single crystal XRD measurement, the many degrees of freedom of the sample stage are necessary. The rotational angles of the sample stage are shown in figure 8 and measured in the following ways:

ω-angle: Angle between incident beam and sample . Measured from y-axis in yz-plane.

χ-angle: Sample stage rotation angle around y-axis in xz-plane. Measured from x-axis.

ϕ-angle: Sample stage rotation angle around z-axis in xy-plane. Measured from y-axis.

2θ-angle: Angle between incident beam and diffracted beam. Measured from y-axis in yz-plane like θ.

[(6)] the K_α is actually split into two levels but due to the small energy difference between the lines we are not able to resolve the difference and a weighted mean of the two levels is used as K_α.

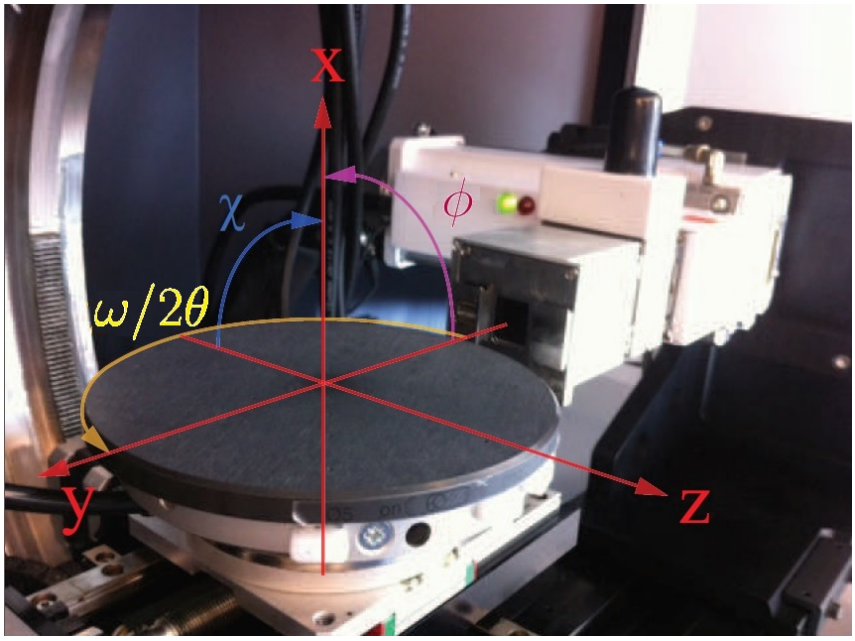

Figure 8: The sample stage where the sample was mounted. After the sample was mounted the sample stage is rotated 90° in the χ direction, i.e. $\chi = 0$ according to the picture. This is done in order to have the surface normal of the sample in the yz-plane.

3.3 X-Ray Diffraction measurements

As the lattice parameters are approximately twice as big for Fe_3O_4 than it is for MgO, a substrate Bragg reflection (hkl) would appear at about the same angle as a $2 \times (hkl)$ film reflection according to (10) and (9). As long as the selection rules for allowed reflections are fulfilled this would thus imply that a Bragg peak of the film is found in the vicinity of a substrate peak. This is a useful relation when finding film peaks as they normally are much weaker than peak from the substrate.

With the Bruker D8 Discover, XRD measurements were applied to investigate properties of the Fe_3O_4/MgO-sample. The studied reflections are given in table 2.

Table 2: Studied reflections.

MgO	(002)	(004)	(224)	-	-
Fe_3O_4	(004)	(008)	(448)	(206)	(026)

Note that the MgO (103) and (013) reflections could not be studied, as odd/even mixed hkl violates the selection rules of allowed reflections in a FCC-lattice. Because of this it is therefore possible to study the Fe_3O_4 (206) and (026) reflections without the influence of the substrate.

Due to the small size of the sample it could not be directly placed on the sample stage. This problem was solved by gluing the sample unto a quadratic glass panel with an appropriate size for the sample stage. In order to be able to orient the sample in the same direction for the different measurements a small line was drawn on one side of the glass

panel shown in figure 9.

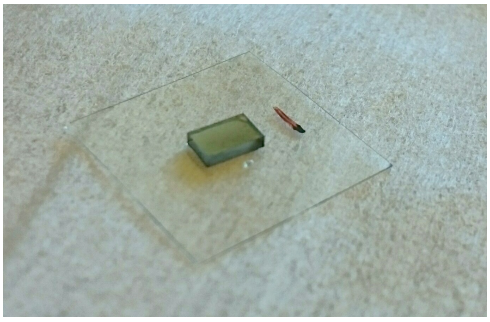

Figure 9: The used sample glued on a marked glass panel showing which side is to be pointing to the X-ray tube.

3.4 Etching process

In order to further analyze the Fe_3O_4 film the MgO substrate has got to be successfully removed. The strategy was to isolate the Fe_3O_4 thin film by chemically etching off the substrate. It is known that a MgO substrate can be completely dissolved by ammonium sulphate $(NH_4)_2SO_4$ according to [12], [13]. Attempts to dissolve the MgO substrate were performed in Lund University Nano Lab.

4 Results

When measuring XRD with Bruker D8 the received data are given in reciprocal space. The intensity of a Bragg peak is measured and as it depends on the Bragg angles for the setup it can be plotted against these angles to give a line-scan plot. It can also be plotted in the vicinity of the peak in two dimensions. This will render a reciprocal space map. In this section the retrieved results from the measurements will be presented as either line scans or reciprocal space maps. Information about the crystal structure can be extracted from these measurements and will also be presented here.

How the scanning directions are related to the reciprocal space may not be intuitive and are therefore graphically illustrated in figure 10. If a reflection is symmetric an incident beam will have the same angle relative to the sample as the outgoing reflected beam and the resulting scattering vector will be parallel to the L-direction.

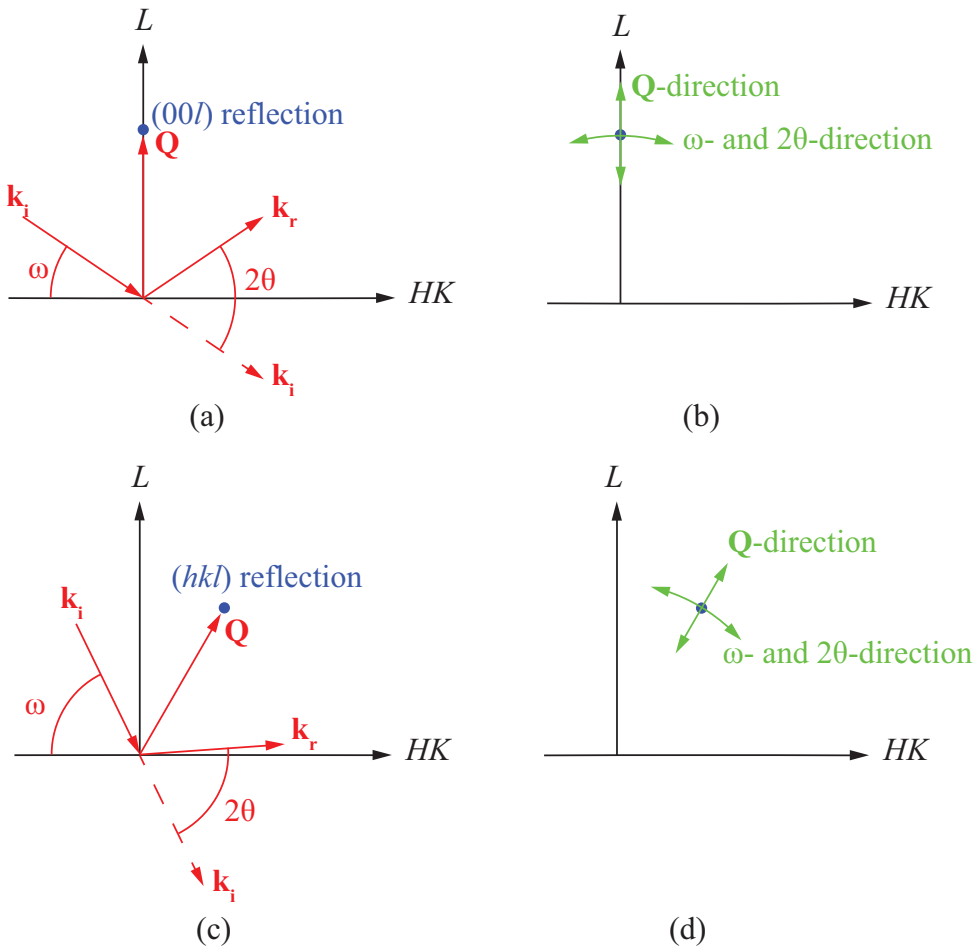

Figure 10: (a) and (c) show two scattering vectors fulfilling the Bragg condition for different reciprocal lattice points. (a) is created by a symmetric reflection. This makes a scan over $\mathbf{Q}$ (an ω-2θ scan) parallel to the L-direction. This is shown in (b). In (c) on the other hand, an asymmetric reflection is shown. In this case a scan over $\mathbf{Q}$ is NOT parallel to L, as shown in (d). Changing only ω or 2θ will make a circular scan with radius $|\mathbf{Q}|$ from the origin in both the symmetric and the asymmetric case.

4.1 Line scans

Different Bragg reflections for both the substrate and the film were investigated and evaluated in certain directions, e.g. along the ω-direction by just pivoting the sample stage or in the 2θ-direction by just moving the detector (see figure 10). As these measurements are one dimensional they can generate a graph with the intensity on the y-axis depending on different angles plotted on the x-axis, hence the name line scan. The directions of the line scan can also be performed over H, K or L in reciprocal lattice units (r.l.u).

For a Bragg peak arising from an ω and its corresponding 2θ-value, a line scan in the direction of the scattering vector $\mathbf{Q}$ can be carried out. This is done by first measuring a set of ω and 2θ and then increasing ω by a set step size at the same time as 2θ is increased by the step size times 2. These scans will be referred to as ω-2θ scans. If a $(00l)$ reflections is considered, the scattering vector will be along the L-direction.

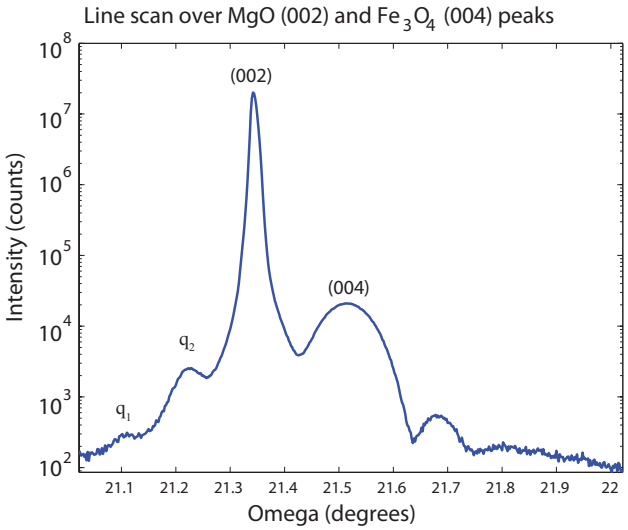

Figure 11: ω-2θ line scan over both substrate (002) and film (004) peaks.

Figure 11 shows such a line scan over two Bragg peaks, one from the substrate MgO and the other for the thin film Fe_3O_4. The substrate peak is very intense and narrow compared to the film peak. This is due to the big differences in layer thickness between the substrate and the film. A thin layer in real space will generate a wide peak in reciprocal space and vice versa. The small bumps in the plot are fringes from the film peak due to Laue oscillations in the out of plane lattice vector $\mathbf{a_3}$.

In figure 12 both the MgO (004) and the Fe_3O_4 (008) peaks are captured in the same line scan. The plot is essentially the same as in figure 11 showing a different order of the reflection. In figure 12 the length between the two Bragg reflections has however increased compared to figure 11. This increase is anticipated as the out of plane lattice parameter a_3 is not exactly twice as big for Fe_3O_4 as it is for MgO. This small difference makes the peaks go further apart with higher orders, i.e. higher hkl.

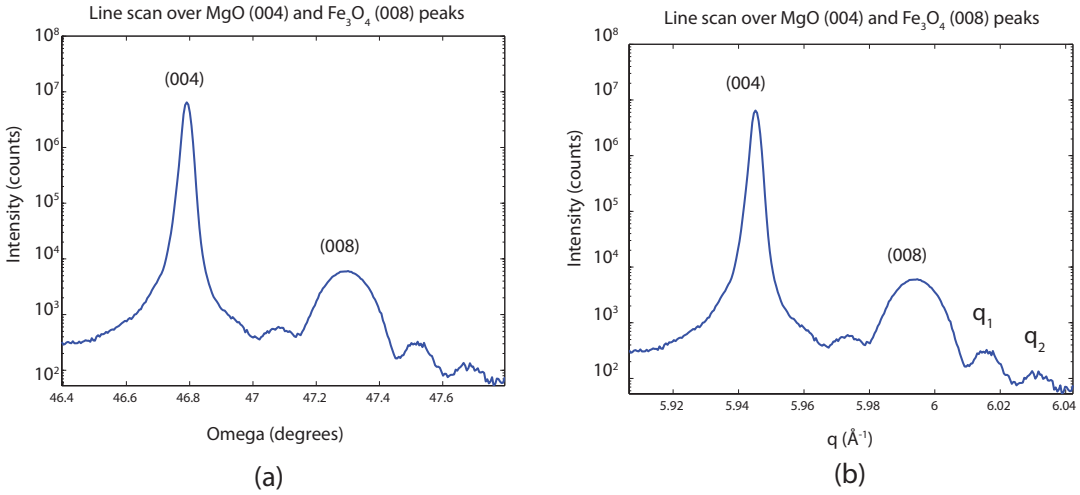

Figure 12: (a) ω-2θ line scan over both substrate (004) and film (008) peaks. The scan was also converted into q in order to calculate the thickness of the film by measuring FWHM of (008) peak and Δq ($q_1 = 6.0158$ Å^{-1}, $q_2 = 6.0298$ Å^{-1}).

By using eq.(12) the ω-2θ scan given in ω was converted into q as shown in figure 12 (b). The obtained FWHM of the peak was 0.0136 Å^{-1} and the distance between q_1 and q_2 was 0.0140 Å^{-1}. By inserting this into eq.(11) and (13) the thickness was estimated to 73.53 Å and 71.43 Å respectively.

The MgO (004) and Fe_3O_4 (008) peaks are also individually evaluated by scanning over ω and keeping the 2θ-value fixed. These types of scans are called ω-scans or rocking curve scans. Because the reflections have different 2θ values the shown figure is superimposed of two different measurements in order to show the difference in width between the two. The retrieved results of the two scans are presented in figure 13 where the x-axis gives the relative ω-angle compared to each peaks maxima.

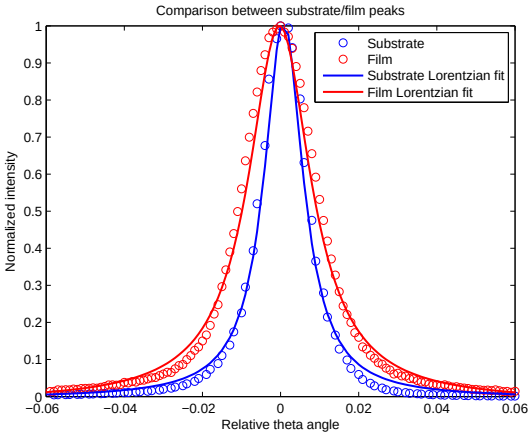

Figure 13: Data from rocking curve scans over substrate peak (004) and film peak (008). The obtained FWHM for the substrate is 0.0123° and for the film 0.0192°.

4.2 Reciprocal space maps

By adding one dimension to regular line scan measurements, i.e. by assembling several line scans next to each other makes it possible to create a landscape over a Bragg reflection. The obtained plot is then called a reciprocal space map or alternatively a mesh scan where the peak can be viewed from a two dimensional perspective.

The Bragg reflection for Fe_3O_4 (206) obeys the selection rules for the film given by table 1. This reflection corresponds to the MgO (103) reflection. However, the (103) reflection violates the selection rules for a FCC lattice as 1 and 3 are odd integers while 0 is considered to be an even. This implies that there are no substrate peak close to the (206) film peak shown in figure 14. The mesh scan shows the Bragg peak relative to the h and l Miller indices keeping k=0 constant. The colorbar to the right displays the intensity (counts at the detector). The intensity is quite low for this peak compared to other Bragg peaks.

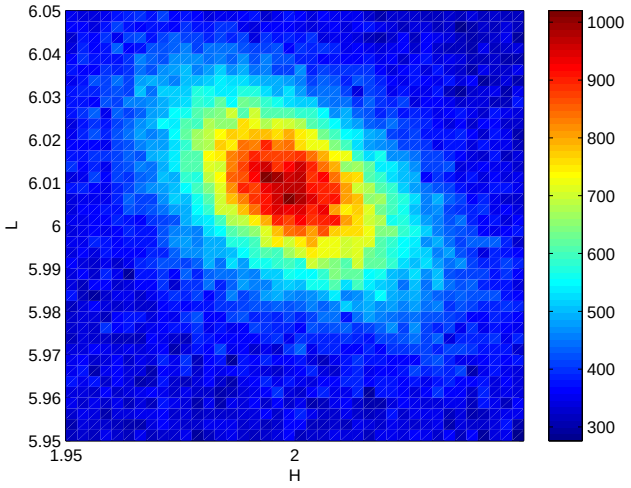

Figure 14: Mesh scan of asymmetric (206) film reflection.

The Fe_3O_4 (026) reflection was also found and measured by rotating the sample stage (ϕ in figure 8) by 90° relative to the (206) reflection. The peak is shown in figure 15. Although the intensity is even lower than the (206) reflection the figure clearly shows a distinct peak.

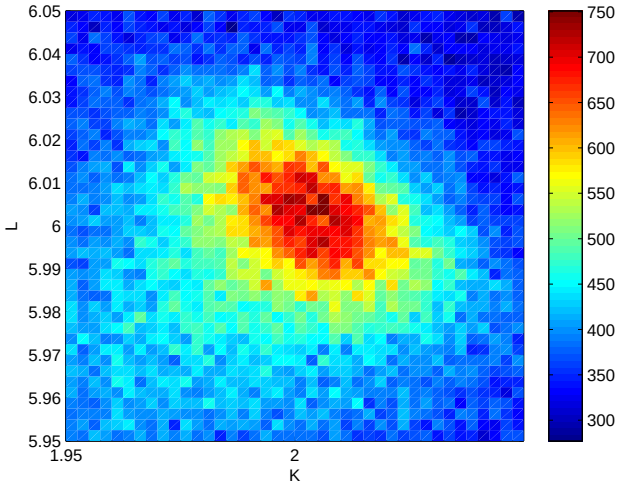

Figure 15: The film (026) reflection.

Neither of the measured asymmetrical reflections (figures 14, 15) show any traces of being split or having double Bragg peaks. This would be expected from tetragonal and orthorhombic structures where $a_1 \neq a_2 \neq a_3$. These measurements therefore concludes that the film is close to the expected cubic structure.

The asymmetric reflection (448) of the film is shown besides the very intense (224) substrate peak in figure 16. The y-axis in the plot is given in L while the x-axis is simultaneously given in both H and K.

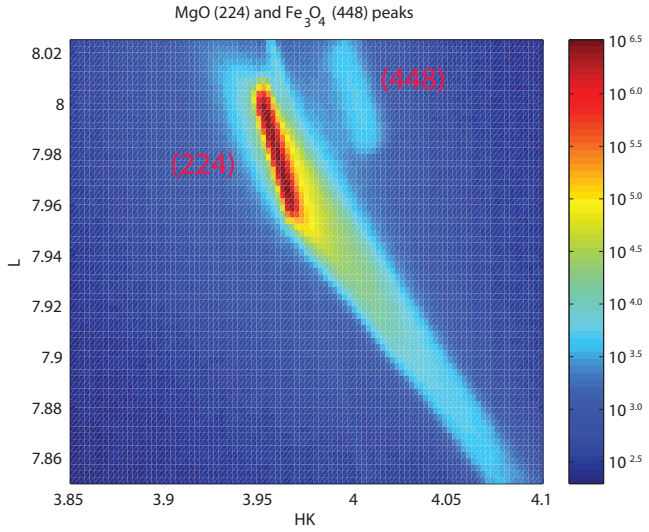

Figure 16: MgO (224) and Fe_3O_4 (448)

The figure again shows that there is a slight difference in both the in-plane and out of plane lattice parameters between the film and substrate. Relative to the MgO lattice parameter, the in-plane lattice parameters appear to be about 0.01% smaller. This is a good indication of that the lattice parameters of the film is relaxed. The reason why the substrate peak is diagonally smeared out could however not be determined and would demand further analysis.

4.3 Dissolving of MgO substrate

Two attempts to dissolve MgO by ammonium sulphate $(NH_4)_2SO_4$ was carried out. In the first attempt 10 grams of $(NH_4)_2SO_4$ was solved in 90 ml of distilled water. A sample of pure MgO super-glued on a SiN-membrane was then dropped down in the solution and heated up to 75° C. By occasionally stirring the solution it was left to vanish on its own under supervision. However, after approximately 3 hours no visible change could be observed other than that the MgO sample had been separated from the SiN-membrane. The sample was left 3 days in the solution at room temperature but even then no change could be detected.

In the second attempt three samples were used, two MgO samples and the investigated Fe_3O_4 thin film sample. A similar solution as in the first attempt was mixed and before samples were sank down into it they were carefully weighed. They were heated up to 75° C for 2 hours, left for two days in room temperature, then reheated up to 75° C again for 1 hour before taken out. After the treatment the samples were weighed again and all three samples could be confirmed to have lost weight. The weight loss is given in table 3.

Table 3: The measured weights of the three samples before and after dissolving attempts.

Sample	Original weight [g]	Weight after treatment [g]	Weight loss [g]
Fe_3O_4	0.0586	0.0555	0.0031
MgO (1)	0.0812	0.0733	0.0079
MgO (2)	0.0901	0.0826	0.0075

In the solution after the second attempt there seemed to be a couple of small metallic pieces/grains smaller than a suger grain floating around. This could possibly be bits Fe_3O_4 from the thin film. However, the film could be confirmed to still be on the substrate with XRD measurements and figure 17 shows a Bragg peak comparison before and after etching attempt on the sample.

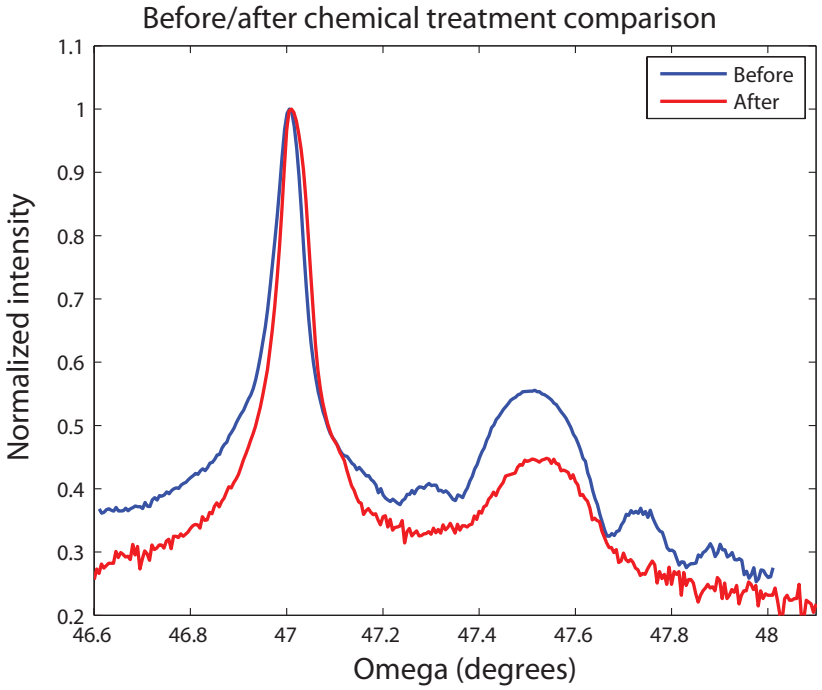

Figure 17: MgO (004) and Fe_3O_4 (008) peaks after treatment in $(NH_4)_2SO_4$. The Fe_3O_4 peak has reduced in intensity compared to the MgO peak. This suggests that the Fe3O4 film may have become damaged during the etching process. More work might be needed to investigate this.

4.4 Calculated values

The Bragg angles for the different measurements are presented in table 4.

Table 4: The measured Bragg angles θ from the different reflections.

Reflection	(004)	(008)	(206)	(026)
θ [°]	21.6259	47.4825	35.5813	35.5871
	-	47.4978	35.5610	-
	-	47.5008	-	-
mean value	21.6259	47.4937	35.5711	35.5871

With the values given in table 4 the lattice parameters for the thin film were calculated using eq. (14), (15), (16). The thickness of the film was also estimated by inserting the difference in q from figure 12 in eq. (11) and by using the measured FWHM from the Fe_3O_4 (004) and (008) reflections and inserting them in eq. (13). The results from this is given in table 5.

Table 5: Calculated properties of the film.

Bragg peak	(004)	(008)	(206)	(026)	mean value
T_{fringe} [Å]	67.57	71.43	-	-	69.47
T_{fwhm} [Å]	75.19	73.53	-	-	74.36
a_3 [Å]	8.360	8.385	-	-	8.372
a_1 [Å]	-	-	8.435	-	8.435
a_2 [Å]	-	-	-	8.402	8.402

5 Discussion and conclusion

5.1 Discussing the data

Characterization of a Fe_3O_4 thin film grown on a MgO substrate was successfully performed using XRD. By analyzing retrieved line/mesh scans in reciprocal space the lattice parameters of the thin film could be verified. It could also be concluded that the thin film had a cubic crystal structure as expected and that the in-plane lattice parameters were relaxed. The thickness of the film could also be approximated by measuring the fringes and the FWHM of symmetric film peaks. Furthermore, the film appears to be of good quality in terms of cations and oxidation errors in the growing process. The film seems indeed to be Fe_3O_4 with good crystalline quality.

The retrieved lengths for the lattice parameters are a_1=8.435 Å, a_2=8.402 Å and a_3=8.372 Å. Compared to the expected bulk value of a=8.399 Å, the calculated values are in good agreement. The small deviations from the expected value in these measurements are

probably due to low statistics. As the number of times the X-ray diffractometer could be used was restricted and some of the asymmetric peaks were difficult to find, the statistics for the measurements were unfortunately also restrained. The theory that the lattice parameters in our measurements were cubic can however be validated. As none of the mesh scans shows any sign of splittings or double Bragg peaks the lattice parameters should be close to equal in lenght, dispite the difference between them according to table 5.

Comparing the width of the MgO (004) with the Fe_3O_4 (008) peak (figure 13) it is noticeable that the FWHM for the two peaks does not differ by that much. The difference in FWHM between the peaks is only 0.0069°. A narrower peak was indeed expected from the substrate as in the case of diffraction by a grating, the peaks grow sharper and narrower the more crystal layers that contribute to the Bragg reflection. The peaks also gets sharper with the quality of the crystal and as our film is very thin it implies that it is of good crystalline quality.

As seen in figures 11 and 12 there are fringes created from the Fe_3O_4 film in the L-direction. By measuring these fringes (and also the FWHM of the symmetric Bragg peaks) an estimation of the thickness of the film could be deduced. The data states that the thickness of the film is about 70 Å. This thickness was retrieved whether the fringes or the FWHM of the film was evaluated. The film could be hence be determined to be thinner than originally expected. From the line scans it could also be observed that the fringes faded away into the background rather quickly. The fading of the fringes is thought to be due to a quite rough interface between the film and the substrate in our particular sample.

Some of the inconsistencies can possibly be from the calibration process of the Bruker D8 (the instrument used for the XRD measurements). The instrument had to be calibrated each time before usage and small divergences from aligning the detector (2θ angle) values between uses could generate a small systematic error. The instrument also proved to be very sensitive as it broke down several times and had to be repaired. It is possible that this might have affected our measurements in some way as well.

According to the references [12] and [13] their Fe_3O_4 thin films could successfully be separated from a MgO substrate by dissolving it using $(NH_4)_2SO_4$. But as a description on how these procedures were carried out is omitted in these studies, we had to try dissolving MgO by simply sinking test samples, as well as our investigated thin film sample, into a solution of $(NH_4)_2SO_4$ and distilled water. Although we did observe weight losses in the samples after they were put into the solution, the reaction was far slower than anticipated and due to time restrictions a successful film-lift off could not be achieved. One likely reason for the slow process might be that our samples were simply larger than the samples used in [12] and [13] prolonging the reaction. A faster reaction might be obtainable by adding more $(NH_4)_2SO_4$ making a stronger solution. But if a stronger concentration is to be used, considerations of how it might affect the film must be taken into account.

5.2 Future goals

In order to understand the mysterious metal to insulator transition in complex metal oxides such as Fe_3O_4, further research is necessary. Understanding this phenomenon could possibly lead to optimization possibilities in technical devices. It may even lead to cur-

rently unknown applications. There are for instance other materials with similar metal to insulator transitions that are already exploited in technology. One example is the material VO_2 which is used as a coating in "smart windows". Smart windows have the ability to be transparent to radiation of certain wavelengths while being opaque to others, depending on its temperature. For VO_2 this transition occurs at room temperature and lets visible light through while infra red light is kept out. This way a room installed with a smart window is able to prevent excessive warming of the room and effectively preserves comfortable room temperature.

To be able to successfully isolate a Fe_3O_4 thin film from a MgO substrate in a future experiment, it might be neccessary to find a different etchant as the one used in this project had an etch rate too. It might also be a good idea to have access to several samples and prioritizing the etching experiments from the start as XRD measurements has much higher success rates.

References

[1] John B. Carlson. Lodestone compass: Chinese or olmec primacy?: Multidisciplinary analysis of an olmec hematite artifact from San Lorenzo, Veracruz, Mexico. *Science*, 189(4205):753–760, 1975.

[2] J. E. Lorenzo, C. Mazzoli, N. Jaouen, C. Detlefs, D. Mannix, S. Grenier, Y. Joly, and C. Marin. Charge and orbital correlations at and above the verwey phase transition in magnetite. *Physical Review Letters*, 101(22):226401, 2008.

[3] Bertram Eugene Warren. *X-ray diffraction*. Addison-Wesley series in metallurgy and materials. Reading, Mass. : Addison-Wesley, 1969.

[4] Philip Hofmann. *Solid State Physics: An Introduction*. Weinheim: WILEY-VCH Verlag GmbH & Co. KGaA, 2011.

[5] Abraham Taylor. *An introduction to X-ray metallography*. London: Chapman & Hall, 1945.

[6] University of Cambridge. *http://www.doitpoms.ac.uk/tlplib/brillouin_zones/reciprocal.php*. verified 2015-04-13.

[7] Gerardina Carbone. *Structural and magnetic studies of strained thin films of* $La_{2/3}Ca_{1/3}MnO_3$. Ph.D Thesis, Max Planck Institute, Stuttgart, 2004.

[8] Nobelprize.org, *http://www.nobelprize.org/nobel_prizes/physics/laureates/1915/wh-bragg-facts.html*. verified 2015-05-11.

[9] University of London Birkbeck College. *http://img.chem.ucl.ac.uk/sgp/large/227bz2.htm*. verified 2015-04-16.

[10] Stephan Geprägs. *Magnetoelectric interactions in multiferroic thin films and composites*. 2011.

[11] Bruker webpage. *https://www.bruker.com/products/x-ray-diffraction-and-elemental-analysis/x-ray-diffraction/components/xrd-components/optics.html*. verified 2015-04-14.

[12] S. Celotto, W. Eerenstein, and T. Hibma. Characterization of anti-phase boundaries in epitaxial magnetite films. *The European Physical Journal B - Condensed Matter and Complex Systems*, 36(2):271–279, 2003.

[13] Zuqin Liu, Daihua Zhang, Song Han, Chao Li, Bo Lei, Weigang Lu, Jiye Fang, and Chongwu Zhou. Single crystalline magnetite nanotubes. *Journal of the American Chemical Society*, 127(1):6–7, 2005.

A Appendix A

Lattice parameters

For orthorhombic crystals the following relation is valid:

$$\frac{1}{d_{hkl}^2} = \frac{h^2}{a_1^2} + \frac{k^2}{a_2^2} + \frac{l^2}{a_3^2} \tag{1}$$

Together with Bragg (10) the planar distance d_{hkl} can be written as:

$$d_{hkl} = \left(\frac{h^2}{a_1^2} + \frac{k^2}{a_2^2} + \frac{l^2}{a_3^2}\right)^{-1/2} = \frac{\lambda}{2\sin\theta} \tag{2}$$

For a $00l$ reflection a_3 can be solved for as:

$$d_{00l} = \frac{a_3}{l} = \frac{\lambda}{2\sin\theta} \tag{3}$$

$$\iff \qquad a_3 = \sqrt{d_{00l}^2 l^2} = \frac{l\lambda}{2\sin\theta} \tag{4}$$

If a_3 already is known from a $00l$ reflection the lattice parameter a_1 can be calculated for a $h0l$ reflection as:

$$d_{h0l}^2 = \left(\frac{h^2}{a_1^2} + \frac{l^2}{a_3^2}\right)^{-1} = \left(\frac{\lambda}{2\sin\theta}\right)^2 \tag{5}$$

$$\iff \qquad h^2 = a_1^2\left(\left(\frac{2\sin\theta}{\lambda}\right)^2 - \frac{l^2}{a_3}\right) \tag{6}$$

$$\iff \qquad a_1 = h\left(\left(\frac{2\sin\theta}{\lambda}\right)^2 - \frac{l^2}{a_3^2}\right)^{-1/2} \tag{7}$$

And analogously to this, for a $0kl$ reflection a_2 can be solved for by:

$$a_2 = k\left(\left(\frac{2\sin\theta}{\lambda}\right)^2 - \frac{l^2}{a_3^2}\right)^{-1/2} \tag{8}$$

Face-Centered-Cubic (FCC) structure factor selection rules

A FCC-lattice unit cell contains four atoms. By taking one of the corner atoms in the FCC-lattice unit cell as the origin the four atoms would have the following co-ordinates; $(0,0,0)$, $(\frac{1}{2},\frac{1}{2},0)$, $(\frac{1}{2},0,\frac{1}{2})$ and $(0,\frac{1}{2},\frac{1}{2})$, see figure 2. For arguments sake we also say that the scattering factor f_n is equal for all atoms in the unit cell. By inserting this into (17) one obtains:

$$F(hkl) = f\left(e^{2\pi i(0+0+0)} + e^{2\pi i(h/2+k/2+0)} + e^{2\pi i(h/2+0+l/2)}e^{2\pi i(0+k/2+l/2)}\right) \tag{9}$$

$$= f\left(1 + e^{\pi i(h+k)} + e^{\pi i(h+l)} + e^{\pi i(k+l)}\right) \tag{10}$$

$$\tag{11}$$

Because hkl all are integers, the sum of any combination of them is also an integer. And since,

$$e^{\pi i n} = \begin{cases} +1 & \text{if } n \text{ is an even integer;} \\ -1 & \text{if } n \text{ is an odd integer.} \end{cases}$$

the structure factor for a FCC-lattice becomes:

$$F(hkl) = \begin{cases} 4f & \text{if } h,k,l \text{ are either all odd or all even;} \\ 0 & \text{if } h,k,l \text{ are mixed.} \end{cases}$$

In other words, the reflection completely cancels out if hkl are mixed. If they either are all even, or all odd, the structure factor becomes $4f$. All allowed reflections therefore yields the same intensity in the FCC-case.